



Radiation Effects on the Flow of Powell-Eyring Fluid Past an Unsteady Inclined Stretching Sheet with Non-Uniform Heat Source/Sink

Tasawar Hayat^{1,3}, Sadia Asad^{1*}, Meraj Mustafa², Ahmed Alsaedi³

1 Department of Mathematics, Quaid-i-Azam University, Islamabad, Pakistan, **2** School of Natural Sciences (SNS), National University of Sciences and Technology (NUST), Islamabad, Pakistan, **3** Department of Mathematics, Faculty of Science, King Abdulaziz University, Jeddah, Saudi Arabia

Abstract

This study investigates the unsteady flow of Powell-Eyring fluid past an inclined stretching sheet. Unsteadiness in the flow is due to the time-dependence of the stretching velocity and wall temperature. Mathematical analysis is performed in the presence of thermal radiation and non-uniform heat source/sink. The relevant boundary layer equations are reduced into self-similar forms by suitable transformations. The analytic solutions are constructed in a series form by homotopy analysis method (HAM). The convergence interval of the auxiliary parameter is obtained. Graphical results displaying the influence of interesting parameters are given. Numerical values of skin friction coefficient and local Nusselt number are computed and analyzed.

Citation: Hayat T, Asad S, Mustafa M, Alsaedi A (2014) Radiation Effects on the Flow of Powell-Eyring Fluid Past an Unsteady Inclined Stretching Sheet with Non-Uniform Heat Source/Sink. PLoS ONE 9(7): e103214. doi:10.1371/journal.pone.0103214

Editor: Gongnan Xie, Northwestern Polytechnical University, China

Received: January 30, 2014; **Accepted:** June 28, 2014; **Published:** July 29, 2014

Copyright: © 2014 Hayat et al. This is an open-access article distributed under the terms of the Creative Commons Attribution License, which permits unrestricted use, distribution, and reproduction in any medium, provided the original author and source are credited.

Funding: This paper was funded by the Deanship of Scientific Research (DSR), King Abdul-Aziz University, Jeddah under grant no. (10 – 130/1434HiCi). The authors, therefore, acknowledge with thanks DSR technical and financial support. The funders had no role in study design, data collection and analysis, decision to publish, or preparation of the manuscript.

Competing Interests: The authors have declared that no competing interests exist.

* Email: asadsadia@gmail.com

Introduction

The study of boundary layer flow and heat transfer over a stretching sheet has gained considerable attention due to its numerous practical applications such as paper production, hot rolling, drawing of plastic films, annealing and tinning of copper wires and metal spinning. Wang [1] proposed the problem of unsteady two-dimensional boundary layer flow of liquid film on unsteady stretching sheet. Later Andersson et al. [2] extended Wang's problem for heat transfer effects by considering time-dependent wall temperature. Further Elbashareshy and Bazid [3] investigated the thermal boundary layer in the time dependent flow (occupying a semi-infinite domain) over an unsteady stretching surface. Ishak et al. [4] studied heat transfer over an unsteady stretching permeable surface with prescribed wall temperature. Radiation effects on the flow and heat transfer over an unsteady stretching surface with internal heat generation were analyzed by Abd El-Aziz [5]. Shateyi and Motsa [6] examined the radiation effects on the time dependent flow of liquid film on unsteady stretching sheet with heat and mass transfer. They obtained an analytic solution of the resulting problem by Chebyshev pseudo-spectral collocation method. Tsai et al. [7] investigated the flow and heat transfer over an unsteady stretching surface with non-uniform heat source. Mukhopadhyay [8] numerically analyzed the flow over unsteady permeable stretching sheet with variable suction and time-dependent surface temperature. In this study, the fluid with variable viscosity and variable thermal conductivity was taken into consideration. Analytic solutions for radiation effects on mixed convection flow of Jeffrey fluid and heat transfer past an unsteady stretching sheet were

provided by Hayat et al. [9]. Three dimension elasto-viscous flow over an unsteady stretching sheet has been discussed by Hayat et al. [10]. Mukhopadhyay [11] extended the work [8] for flow near a stagnation-point with variable free stream. MHD stagnation-point flow of an electrically conducting Casson fluid past an unsteady stretching surface was explored by Bhattacharyya [12]. Yang and Baleanu [13] investigated the fractal heat conduction problem. They solved by using local fractional variation iteration method. Yang et al. [14] presented local fractional Fourier series solutions for non-homogeneous heat equations arising in fractal heat flow with local fractional derivative.

It has now been widely recognized that in industrial and engineering applications, non-Newtonian fluids are more suitable than Newtonian fluids. Due to the flow diversity in nature, the rheological features of non-Newtonian fluids cannot be captured by a single constitutive relationship between stress and shear rate. For this reason, a variety of non-Newtonian fluid models (exhibiting different rheological effects) are available in the literature [15,16]. Amongst those is the Powell-Eyring fluid [17] which although mathematically complex has tendency to describe the flow behavior at low and high shear rates. It can be used to formulate the flows of modern industrial materials such as powdered graphite and ethylene glycol. Unidirectional flow of Powell-Eyring fluid between parallel plates with couple stresses was studied by Eldabe et al. [18]. Pulsatile flow of Powell-Eyring fluid was examined by Zueco and Beg [19]. Homotopy perturbation analysis of slider bearing lubricated with Powell-Eyring fluid was presented by Islam et al. [20]. Three-dimensional flow of Powell-Eyring fluid past a wedge was discussed by Patel

and Timol [21]. Boundary layer flow of Powell-Eyring fluid over a moving flat plate was analyzed by Hayat et al. [22]. Recently steady flow of Powell-Eyring fluid over an exponentially stretching sheet was numerically investigated by Mushtaq et al. [23]. It has been noted that literature is scarce for unsteady flow of Powell-Eyring fluid. To our information, the flow and heat transfer of the Powell-Eyring fluid thin film over an unsteady stretching sheet are examined by Khader and Megahed [24]. Impact of uniform suction/injection in unsteady Couette flow of Powell-Eyring fluid is explored by Zaman et al. [25].

The present work considers the boundary layer flow of Powell-Eyring fluid over an unsteady stretching sheet. The stretching sheet is considered inclined. In addition the effects of radiation and non-uniform heat source/sink are also taken into account. Radiative heat transfer in the boundary layer flow is very important from application point of view, because the quality of the final product is very much dependent on the rate of heat transfer of the ambient fluid particles. Such radiative effects are also important in many non-isothermal cases whereas the heat generation/absorption in moving fluids is significant in the applications involving heat removal from nuclear fuel debris, underground disposal of radioactive waste material, storage of food stuffs, dislocating of fluids in packed bed reactors and several others. Similar situations prevail during the manufacture of plastic and rubber sheets where it is often necessary to blow a gaseous medium through the not-yet solidified material, and where the stretching force may be varying with time. The dimensionless mathematical problems are solved analytically by homotopy analysis method (HAM) [26–40]. Homotopy analysis method (HAM) is one of the most efficient methods in solving different type of nonlinear equations such as coupled, decoupled, homogeneous and non-homogeneous. Many previous analytic methods have some restrictions in dealing with nonlinear equations. For illustration, in contrast to perturbation method, HAM is independent of any small or large parameters and or the existence of auxiliary parameter provides us with a simple way to control and adjust the convergence region which is a main lack of previous techniques. Also, HAM provides us with great freedom to choose different initial guesses to express solutions of the nonlinear problem. Numerical values of wall velocity and temperature gradient are computed and examined.

Mathematical Formulation

We consider unsteady two-dimensional incompressible flow of Powell-Eyring fluid past a stretching sheet. The sheet makes an angle α with the vertical direction. The x - and y -axes are taken along and perpendicular to the sheet respectively. In addition the effects of thermal radiation and non-uniform heat source/sink are considered (see Fig. 1). The Cauchy stress tensor in Powell-Eyring fluid is given by [17]:

$$\tau_{ij} = \mu \frac{\partial u_i}{\partial x_j} + \frac{1}{\beta} \sinh^{-1} \left(\frac{1}{C} \frac{\partial u_i}{\partial x_j} \right),$$

where μ is the viscosity coefficient, β and C are the material fluid parameters. The boundary layer equations comprising the balance laws of mass, linear momentum and energy can be written as [19–26]

$$\frac{\partial u}{\partial x} + \frac{\partial v}{\partial y} = 0, \tag{1}$$

$$\begin{aligned} \frac{\partial u}{\partial t} + u \frac{\partial u}{\partial x} + v \frac{\partial u}{\partial y} = \\ \left(v + \frac{1}{\rho \tilde{\beta} C} \right) \frac{\partial^2 u}{\partial y^2} - \frac{1}{2\rho \tilde{\beta} C^3} \left(\frac{\partial u}{\partial y} \right)^2 \frac{\partial^2 u}{\partial y^2} + g_0 \beta_T (T - T_\infty) \cos \alpha, \end{aligned} \tag{2}$$

$$\rho c_p \left[\frac{\partial T}{\partial t} + u \frac{\partial T}{\partial x} + v \frac{\partial T}{\partial y} \right] = k \frac{\partial^2 T}{\partial y^2} - \frac{\partial q_r}{\partial y} + q''. \tag{3}$$

In the above expressions t is the time, $\nu = (\mu / \rho)$ is the kinematic viscosity, k is the thermal conductivity of the fluid, ρ is the fluid density, T is the fluid temperature, c_p is the specific heat, g_0 is the acceleration due to gravity, β_T is the volumetric coefficient of thermal expansion, $q_r = -\frac{16\sigma^* T_\infty^3}{3k^*} \frac{\partial T}{\partial y}$ [36–38] is the linearized radiative heat flux, k^* is the mean absorption coefficient, σ^* is the Stefan-Boltzmann constant, q'' is the non-uniform heat generated ($q'' > 0$) or absorbed ($q'' < 0$) per unit volume. The non-uniform heat source/sink, q'' is modeled by the following expression [39–40].

$$q'' = \frac{ku_s(x, t)}{xv} [A(T_s - T_\infty)f' + (T - T_\infty)B], \tag{4}$$

in which A and B are the coefficient of space and temperature-dependent heat source/sink, respectively. Here two cases arise. For internal heat generation $A > 0$ and $B > 0$ and for internal heat absorption, we have $A < 0$ and $B < 0$.

The surface velocity is denoted by $u_s(x, t) = \frac{bx}{(1-at)}$ whereas the surface temperature $T_s(x, t) = T_\infty + T_{ref} \frac{bx^2}{2\nu} (1-at)^{-3/2}$. Here b (stretching rate) and a are positive constants having dimension time^{-1} . Also T_{ref} is a constant reference temperature. We note that the temperature of stretching sheet is larger than the free stream temperature T_∞ .

The boundary conditions are taken as follows:

$$u = u_s(x, t), v = 0, T = T_s(x, t) \text{ at } y = 0, \tag{5}$$

$$u \rightarrow 0, T \rightarrow T_\infty \text{ as } y \rightarrow \infty.$$

Introducing

$$\begin{aligned} u = \frac{bx}{(1-at)} f'(\eta), v = -\sqrt{\frac{vb}{(1-at)}} f(\eta), \\ \theta = \frac{T - T_\infty}{T_s - T_\infty}, \eta = \sqrt{\frac{b}{\nu(1-at)}} y, \end{aligned} \tag{6}$$

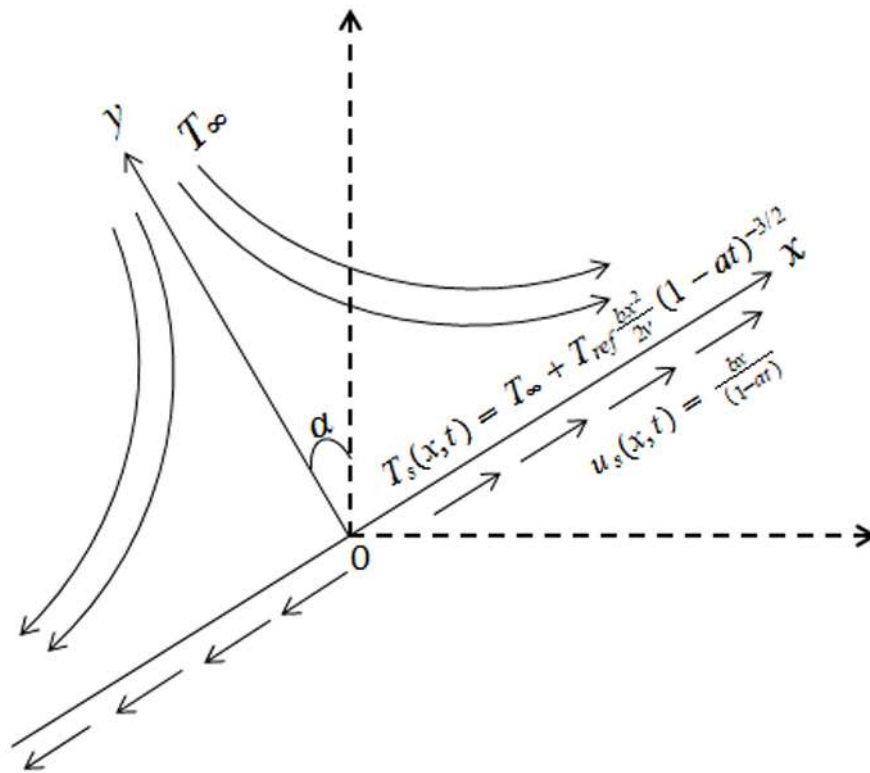


Figure 1. Physical model and coordinate system.
doi:10.1371/journal.pone.0103214.g001

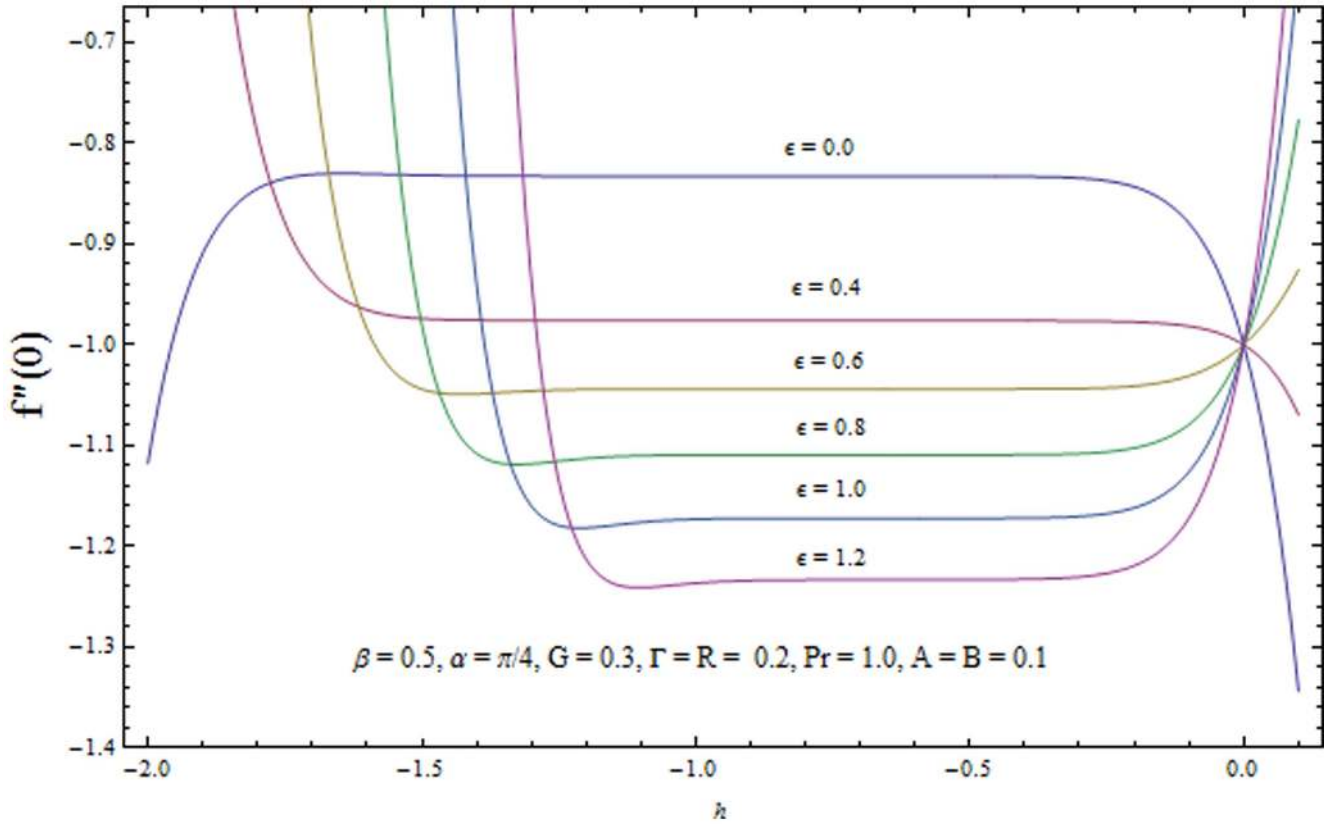


Figure 2. The h -curves for the velocity field.
doi:10.1371/journal.pone.0103214.g002

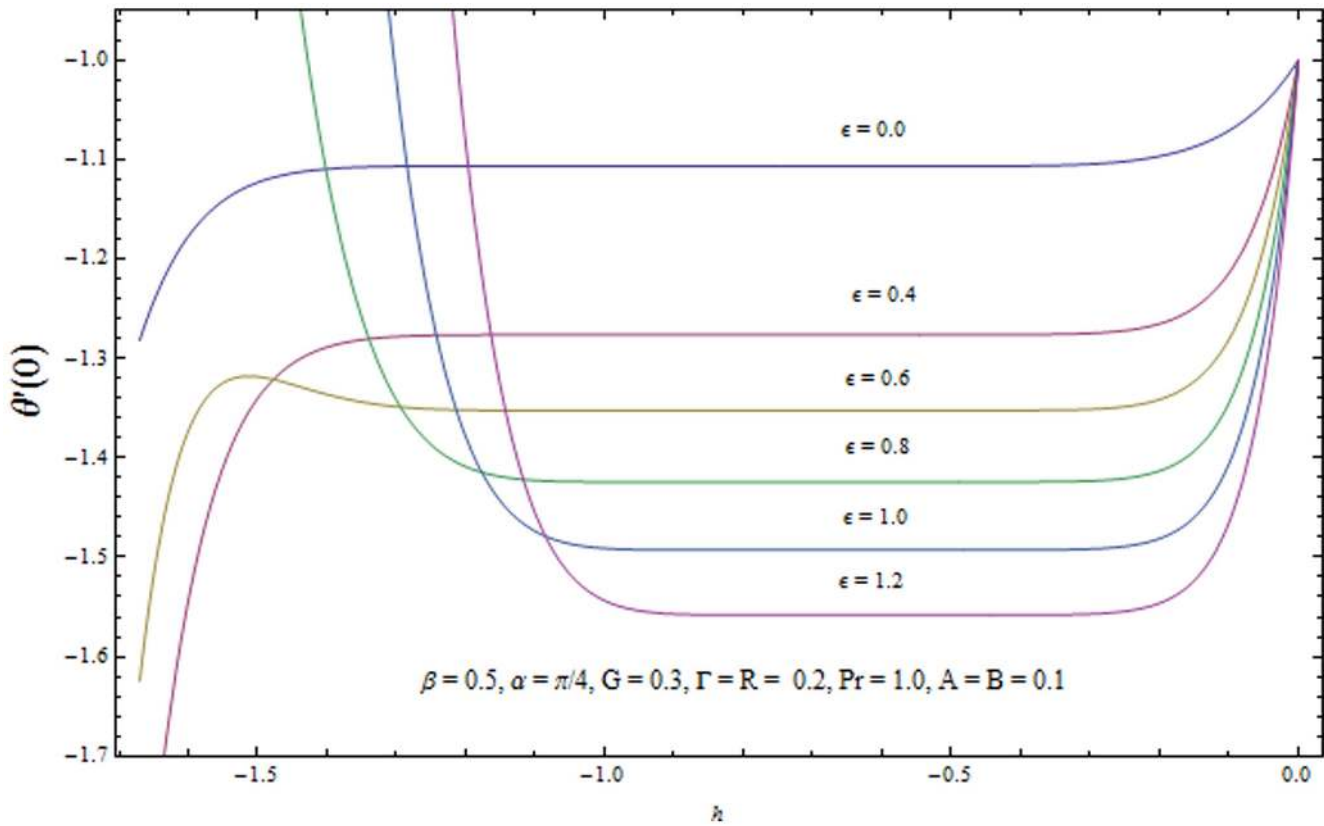


Figure 3. The h -curves for the temperature field.
doi:10.1371/journal.pone.0103214.g003

Eq. (1) is identically satisfied and Eqs. (2)–(5) become

$$(1 + \Gamma)f''' - f'^2 + ff'' - \Gamma\beta f''^2 f''' - \epsilon(f' + \frac{1}{2}\eta f'') + G\theta \cos \alpha = 0, \quad (7)$$

$$\begin{aligned} f = 0, f' = 1, \theta = 1 \text{ at } \eta = 0, \\ f' \rightarrow 0, \theta \rightarrow 0 \text{ as } \eta \rightarrow \infty, \end{aligned} \quad (9)$$

$$\left(1 + \frac{4}{3}R\right)\theta'' + \text{Pr}\left(f\theta' - 2f'\theta - \frac{1}{2}\epsilon(3\theta + \eta\theta')\right) + Af' + B\theta = 0, \quad (8)$$

where prime denotes differentiation with respect to η , f is the dimensionless stream function, θ is the dimensionless temperature and the dimensionless numbers are

Table 1. Convergence of series solutions for different order of approximations when $\alpha = \pi/4$, $\beta = 0.5$, $\Gamma = 0.2$, $R = 0.2$, $\epsilon = 0.6$, $G = 0.3$, $\text{Pr} = 1.0$, $A = B = 0.1$, $h_f = -0.8$ and $h_\theta = -0.7$.

Order of approximation	$-f''(0)$	$-\theta'(0)$
1	1.03515	1.33250
5	1.04402	1.35252
10	1.04401	1.35252
15	1.04401	1.35252
20	1.04401	1.35252
30	1.04401	1.35252

doi:10.1371/journal.pone.0103214.t001

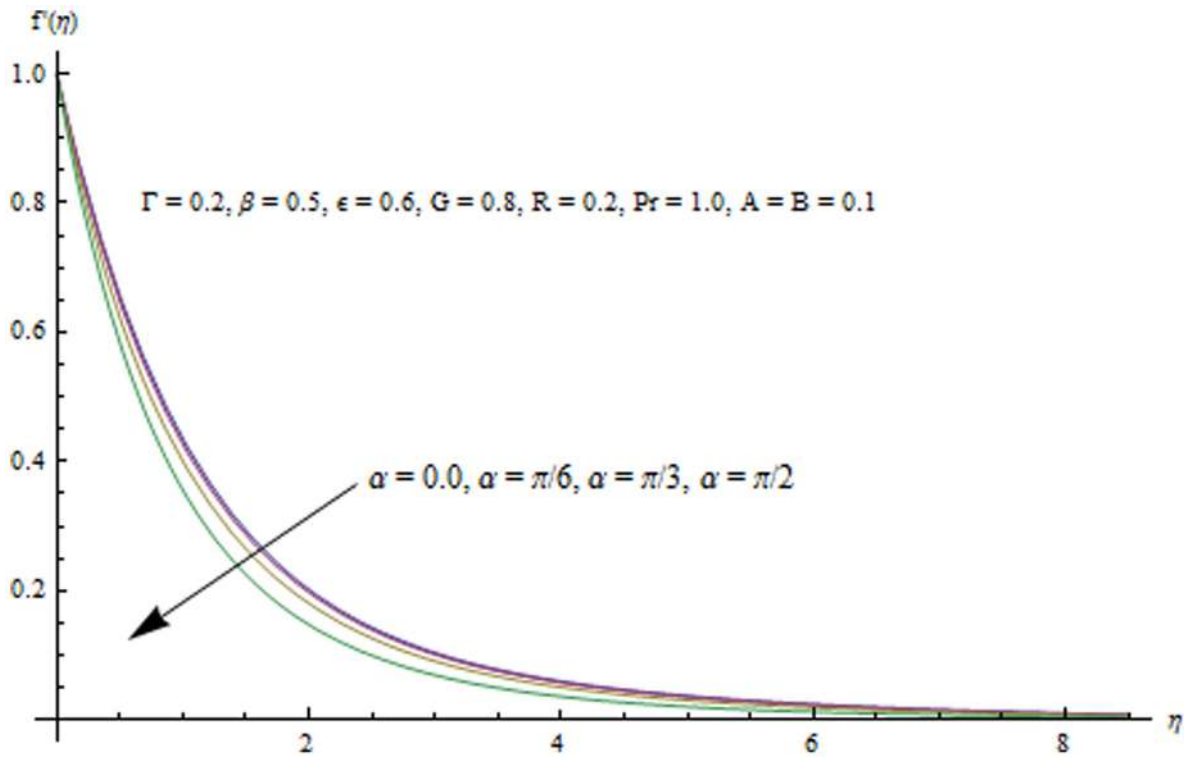


Figure 4. Influence of α on the velocity field.
doi:10.1371/journal.pone.0103214.g004

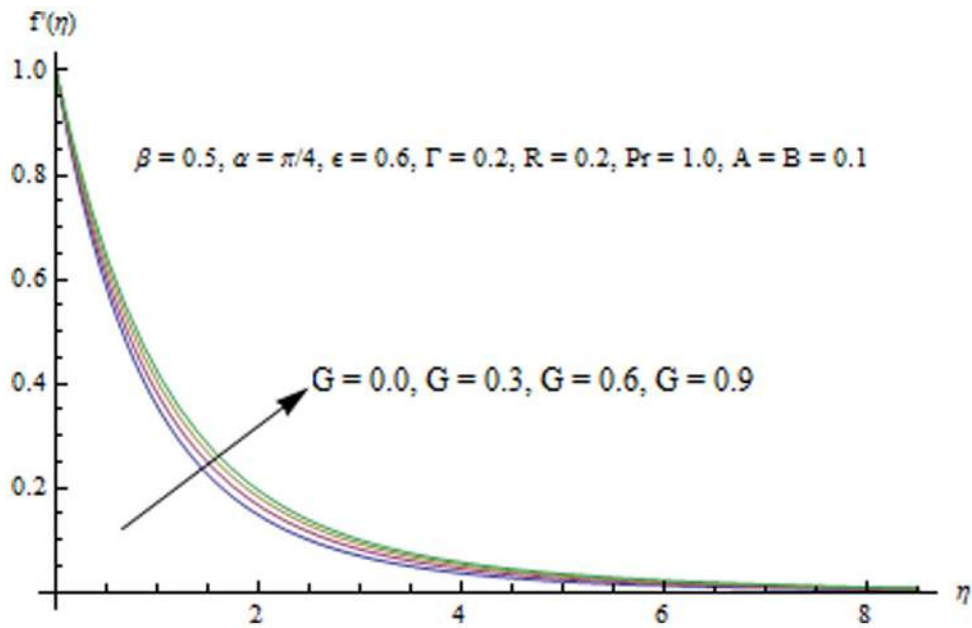


Figure 5. Influence of G on the velocity field.
doi:10.1371/journal.pone.0103214.g005

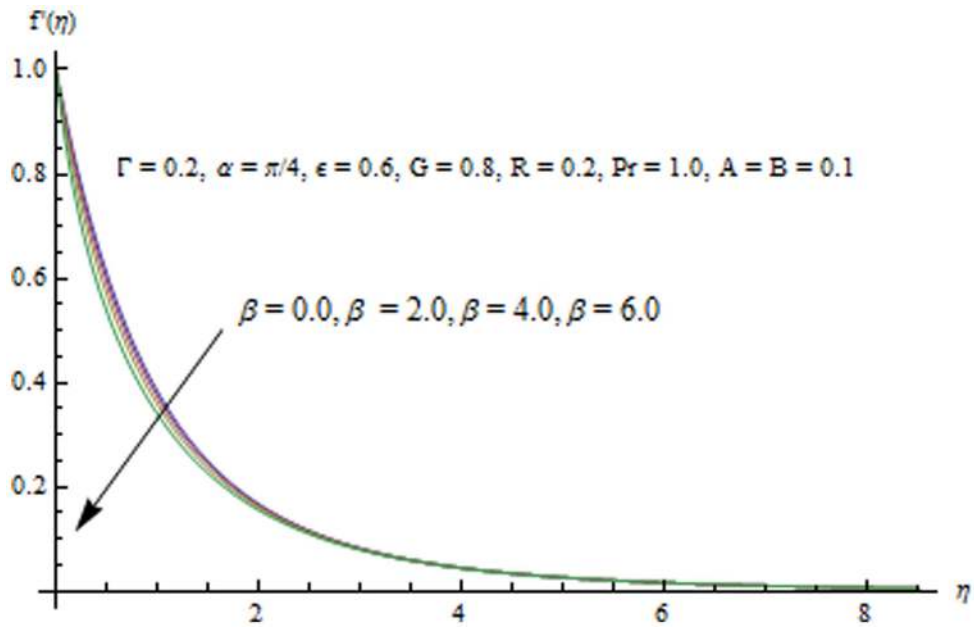


Figure 6. Influence of β on the velocity field.
doi:10.1371/journal.pone.0103214.g006

$$\Gamma = \frac{1}{\mu\tilde{\beta}C}, R = \frac{4\sigma^*T_\infty^3}{kk^*}, \beta = \frac{\rho u_s^3}{\mu x C^2}, \quad (10)$$

$$G = \frac{g\beta_T(T_s - T_\infty)x^3/v^2}{u_s^2 x^2/v^2} = \frac{Gr_x}{Re_x^2}, \epsilon = \frac{a}{b}, Pr = \frac{\mu c_p}{k}.$$

Here Γ and β are dimensionless material fluid parameters, R is the radiation parameter, ϵ is the unsteady parameter and Pr is the Prandtl number.

Local Nusselt number Nu_x is defined as

$$Nu_x = \frac{xq_w}{k(T_w - T_\infty)}; q_w = -k\left(\frac{\partial T}{\partial y}\right)_{y=0} + (q_r)_w, \quad (11)$$

$$Re_x^{-1/2}Nu_x = -\left(1 + \frac{4}{3}R\right)\theta'(0),$$

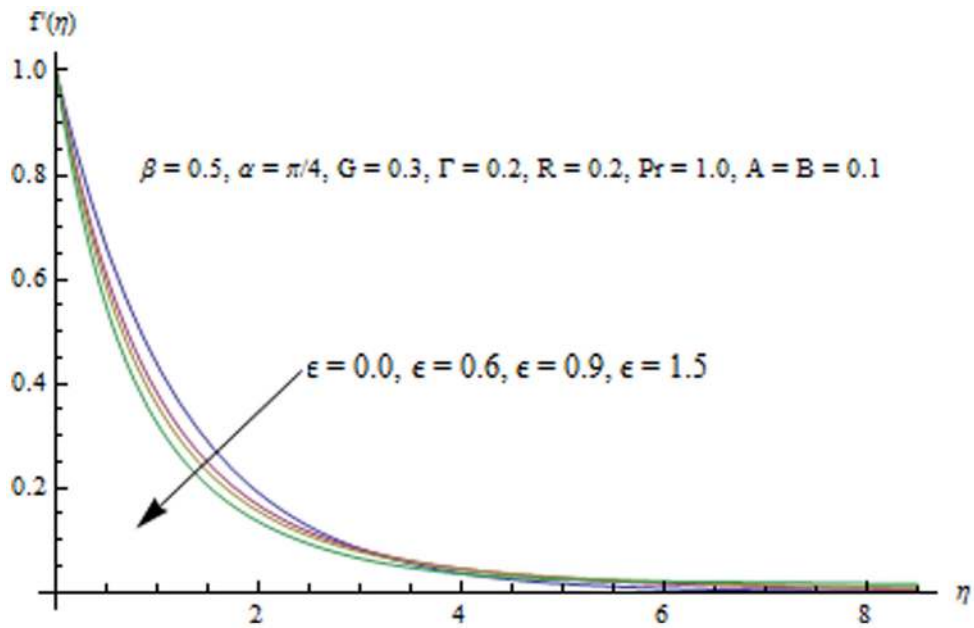


Figure 7. Influence of ϵ on the velocity field.
doi:10.1371/journal.pone.0103214.g007

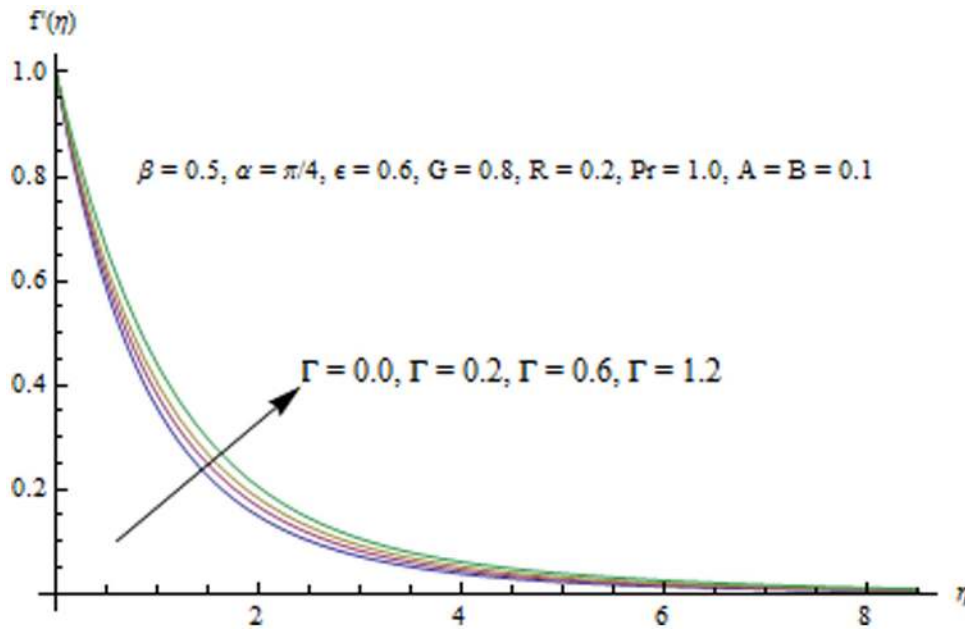


Figure 8. Influence of Γ on the velocity field.
doi:10.1371/journal.pone.0103214.g008

where $Re_x = \frac{u_s X}{\nu}$ is the local Reynolds number.

Solution Methodology

Most of the problems occurring in the field of science and engineering are non-linear. Specifically most of the problems encountered in fluid mechanics are highly non-linear. To find the exact solution of these non-linear problems is very difficult and some times even impossible. Thus several numerical and analytical techniques have been developed to solve such kind of problems.

Among these HAM is the most used analytical technique. Convergent series solutions of non-linear equations are obtained.

Homotopy analysis method

HAM was proposed by means of homotopy, a fundamental concept of topology. Two functions are said to be homotopic if one function can be deformed continuously into the other function. If f_1 and f_2 are two continuous maps from the topological space X into the topological space Y then f_1 is homotopic to f_2 if there exist a continuous map F

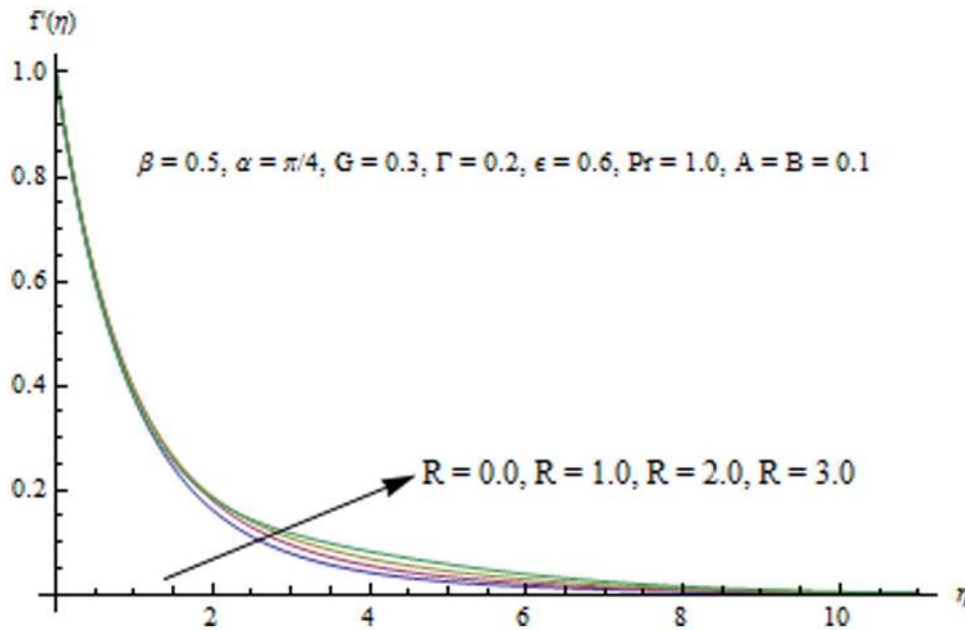


Figure 9. Influence of R on the velocity field.
doi:10.1371/journal.pone.0103214.g009

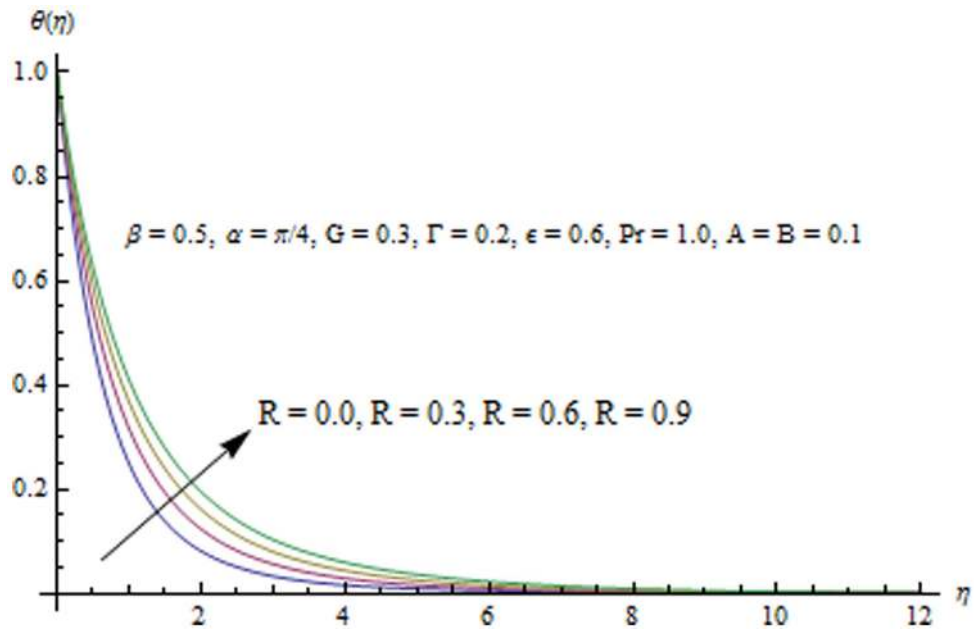


Figure 10. Influence of R on the temperature field.
doi:10.1371/journal.pone.0103214.g010

$$F : X \times [0, 1] \rightarrow Y$$

such that for each $x \in X$

$$F(x, 0) = f_1(x), F(x, 1) = f_2(x)$$

The map F is called homotopy between f_1 and f_2 .

It should be noted that there is a great freedom to choose initial guess and auxiliary linear operator \mathcal{L} . Beside such a great freedom there are some fundamental rules which direct us to choose the mentions parameters in more efficient way. Therefore, initial guesses for the velocity and temperature fields are taken in such a way that they satisfy the boundary conditions given in Eq. (9). And we choose linear operator specified in Eq. (13) that must satisfy the properties given in Eq. (14).

$$f_0(\eta) = 1 - e^{-\eta}, \theta_0(\eta) = e^{-\eta}, \quad (12)$$

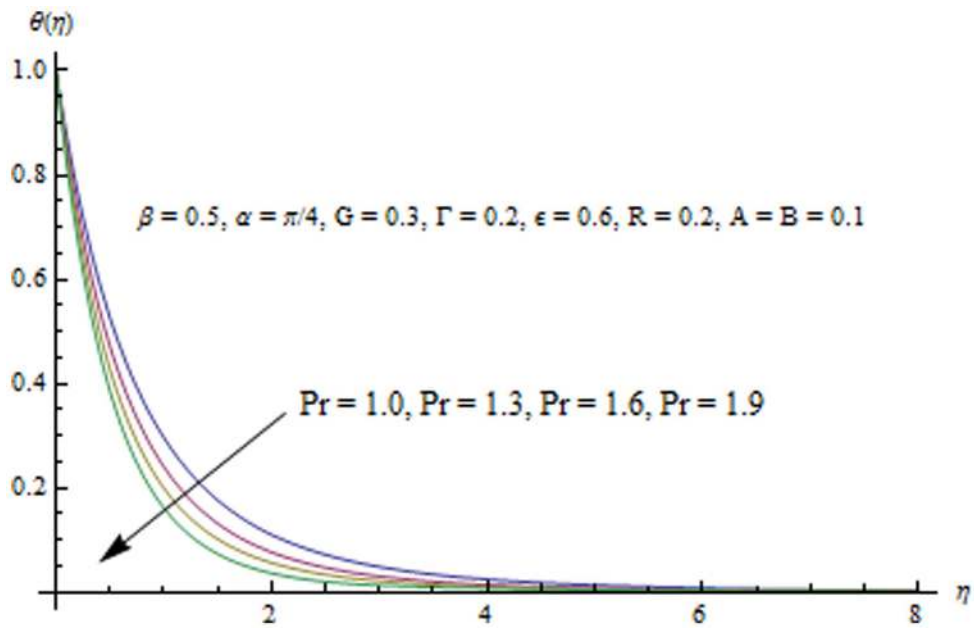


Figure 11. Influence of Pr on the temperature field.
doi:10.1371/journal.pone.0103214.g011

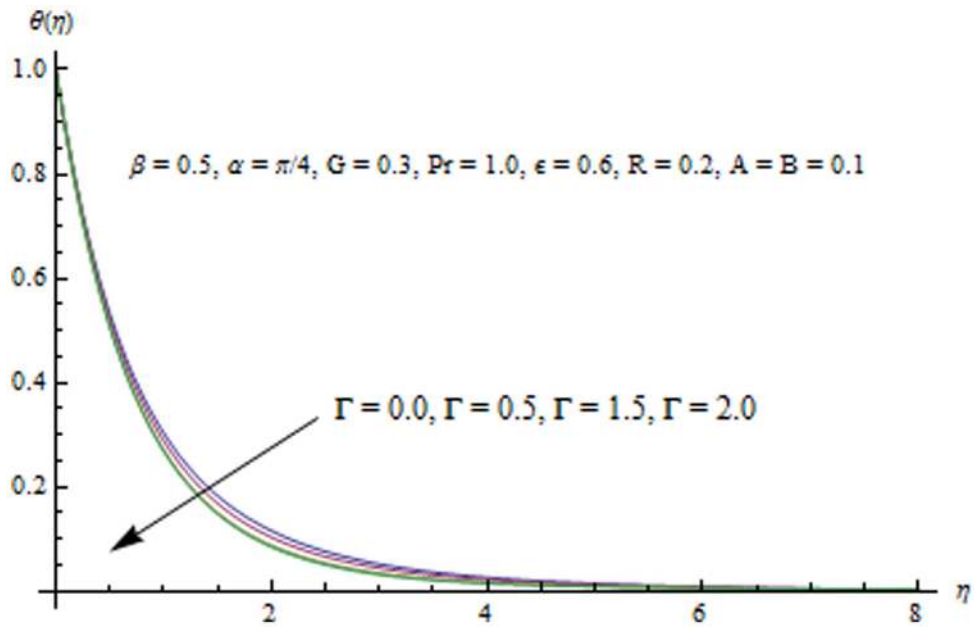


Figure 12. Influence of Γ on the temperature field.
doi:10.1371/journal.pone.0103214.g012

$$\xi_f = f''' - f', \xi_\theta = \theta'' - \theta,$$

subject to the properties

$$\xi_f(C_1 + C_2e^\eta + C_3e^{-\eta}) = 0, \xi_\theta(C_4e^\eta + C_5e^{-\eta}) = 0, \quad (13)$$

where C_i ($i = 1-5$) are the constants.

The deformation problems subjected to zeroth order

$$(1-p)\xi_f[f(\eta;p) - f_0(\eta)] = p h_{ff}[f(\eta;p)], \quad (14)$$

$$(1-p)\xi_\theta[\theta(\eta;p) - \theta_0(\eta)] = p h_{\theta\theta}[\theta(\eta;p)], \quad (15)$$

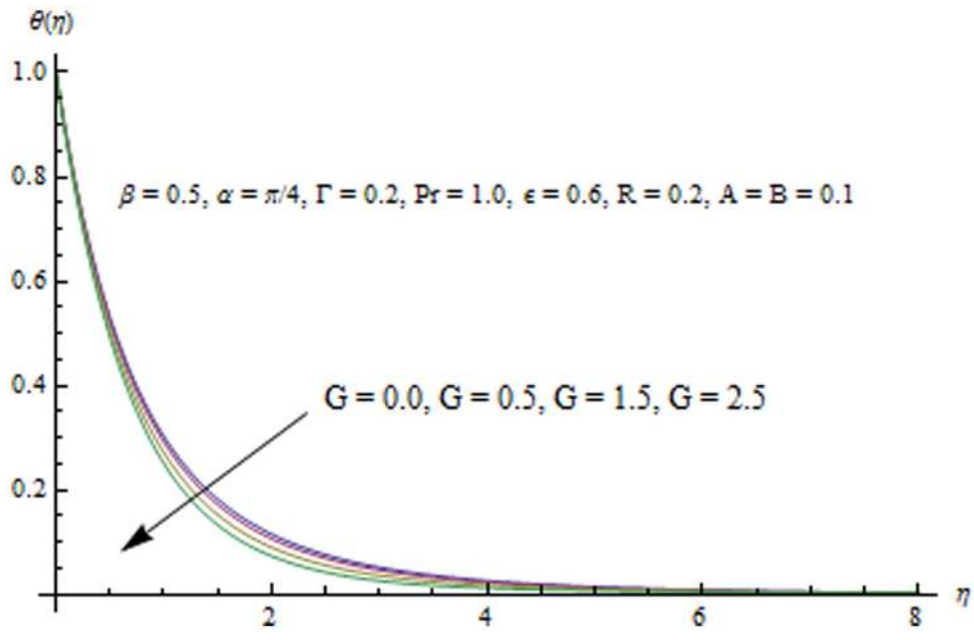


Figure 13. Influence of G on the temperature field.
doi:10.1371/journal.pone.0103214.g013

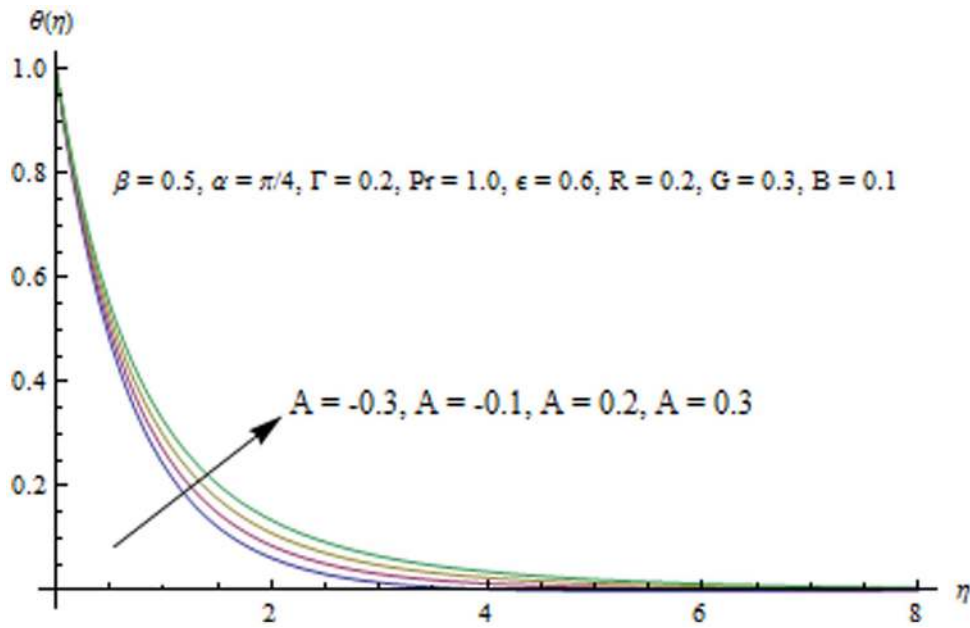


Figure 14. Influence of A on the temperature field.
doi:10.1371/journal.pone.0103214.g014

$$\hat{f}(0; p) = 0, \hat{f}'(0; p) = 1, \hat{f}'(\infty; p) = 0, \hat{\theta}(0; p) = 1, \hat{\theta}(\infty; p) = 0. \quad (16)$$

$$\hat{f}(\eta; 1) = f(\eta), \hat{\theta}(\eta; 1) = \theta(\eta).$$

If $p \in [0, 1]$ indicates the embedding parameter, h_f and h_θ the non-zero auxiliary parameters then the nonlinear differential operators N_f and N_θ are given by

It is noticed that when p varies from 0 to 1 then $f(\eta; p)$ and $\theta(\eta; p)$ approach from $f_0(\eta)$, $\theta_0(\eta)$ to $f(\eta)$ and $\theta(\eta)$. The series of f and θ through Taylor's expansion are chosen convergent for $p = 1$ and thus

$$\begin{aligned} N_f[\hat{f}(\eta; p)] &= (1 + \Gamma) \frac{\partial^3 \hat{f}(\eta; p)}{\partial \eta^3} + \hat{f}(\eta; p) \frac{\partial^2 \hat{f}(\eta; p)}{\partial \eta^2} - \left(\frac{\partial \hat{f}(\eta; p)}{\partial \eta} \right)^2 \\ &- \Gamma \beta \left(\frac{\partial^2 \hat{f}(\eta; p)}{\partial \eta^2} \right)^2 \frac{\partial^3 \hat{f}(\eta; p)}{\partial \eta^3} - \epsilon \left(\frac{\partial \hat{f}(\eta; p)}{\partial \eta} + \frac{1}{2} \eta \frac{\partial^2 \hat{f}(\eta; p)}{\partial \eta^2} \right) \\ &+ G \hat{\theta}(\eta; p) \cos \alpha, \end{aligned} \quad (17)$$

$$f(\eta) = f_0(\eta) + \sum_{m=1}^{\infty} f_m(\eta), f_m(\eta) = \frac{1}{m!} \frac{\partial^m f(\eta; p)}{\partial \eta^m} \Big|_{p=0}, \quad (20)$$

$$\theta(\eta) = \theta_0(\eta) + \sum_{m=1}^{\infty} \theta_m(\eta), \theta_m(\eta) = \frac{1}{m!} \frac{\partial^m \theta(\eta; p)}{\partial \eta^m} \Big|_{p=0}. \quad (21)$$

$$\begin{aligned} N_\theta[\hat{\theta}(\eta; p), \hat{f}(\eta; p)] &= \\ &\left(1 + \frac{4}{3} R \right) \frac{\partial^2 \hat{\theta}(\eta; p)}{\partial \eta^2} + \left[\text{Pr} \hat{f}(\eta; p) \frac{\partial \hat{\theta}(\eta; p)}{\partial \eta} - 2 \hat{\theta}(\eta; p) \frac{\partial \hat{f}(\eta; p)}{\partial \eta} \right. \\ &\left. - \epsilon \left(3 \hat{\theta}(\eta; p) + \eta \frac{\partial \hat{\theta}(\eta; p)}{\partial \eta} \right) \right] + A \frac{\partial \hat{f}(\eta; p)}{\partial \eta} + B \hat{\theta}(\eta; p). \end{aligned} \quad (18)$$

The resulting problems at m^{th} order can be presented in the following forms

$$\mathcal{L}_f[f_m(\eta) - x_m f_{m-1}(\eta)] = h_f R_f^m(\eta), \quad (22)$$

$$\mathcal{L}_\theta[\theta_m(\eta) - x_m \theta_{m-1}(\eta)] = h_\theta R_\theta^m(\eta), \quad (23)$$

We have for $p = 0$ and $p = 1$ the following equations

$$f_m(0) = f'_m(0) = f'_m(\infty) = \theta_m(0) = \theta_m(\infty)$$

$$\hat{f}(\eta; 0) = f_0(\eta), \hat{\theta}(\eta; 0) = \theta_0(\eta), \quad (19)$$

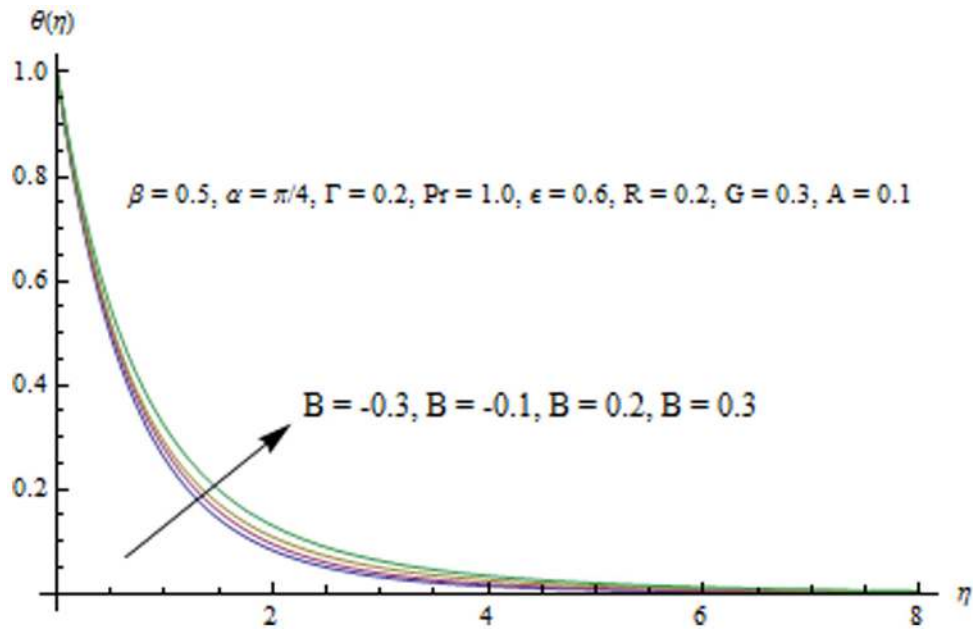


Figure 15. Influence of B on the temperature field.
doi:10.1371/journal.pone.0103214.g015

$$\begin{aligned}
 \mathbf{R}_f^m(\eta) &= (1 + \Gamma) f_{m-1}'''(\eta) \\
 &+ \sum_{k=0}^{m-1} \left[f_{m-1-k} f_k'' - f_{m-1-k}' f_k' - \Gamma \beta f_{m-1}'' \sum_{k=0}^{m-1} f_k'' f_l''' \right] \quad (24) \\
 &- \varepsilon \left(f_{m-1}' + \frac{1}{2} \eta f_{m-1}'' \right) + G \theta_{m-1} \cos \alpha,
 \end{aligned}$$

$$\begin{aligned}
 \mathbf{R}_\theta^m(\eta) &= \left(1 + \frac{4}{3} R_d \right) \theta_{m-1}''(\eta) \\
 &+ \text{Pr} \sum_{k=0}^{m-1} \left[\theta_{m-1-k}' f_k - 2 f_{m-1-k}' \theta_k - \frac{1}{2} \varepsilon (3 \theta_{m-1} + \eta \theta_{m-1}') \right] \quad (25) \\
 &+ A f_{m-1}' + B \theta_{m-1},
 \end{aligned}$$

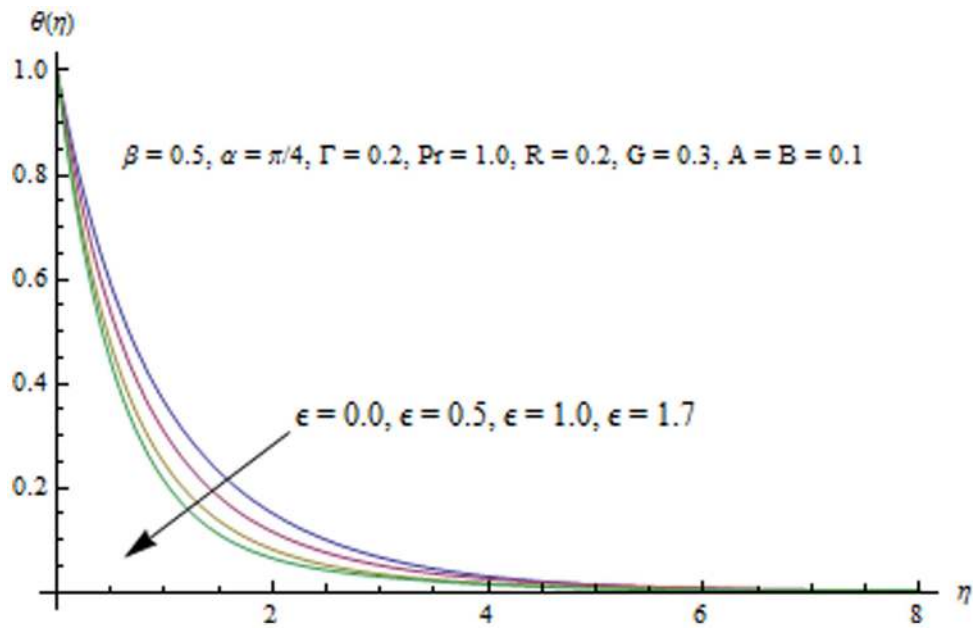


Figure 16. Influence of ε on the temperature field.
doi:10.1371/journal.pone.0103214.g016

Table 2. Comparison between numerical solution Tsai et. al. [7] and HAM solution in a special case when $\alpha = \beta = \varepsilon = \Gamma = G = R = 0$.

Pr	B	A	Present study	Tsai et. [7]
1.0	- 1.0	0.0	- 1.71094	- 1.710937
	- 2.0	- 1.0	- 2.36788	
2.0	- 1.0	0.0	- 2.25987	
	- 2.0	- 1.0	- 2.486000	- 2.485997

doi:10.1371/journal.pone.0103214.t002

$$x_m = 0, m \leq 1, \quad \theta_m(\eta) = \theta_m^*(\eta) + C_4 e^\eta + C_5 e^{-\eta}, \quad (27)$$

$$x_m = 1, m > 0.$$

The general solutions (f_m, θ_m) comprising the special solutions (f_m^*, θ_m^*) are

$$f_m(\eta) = f_m^*(\eta) + C_1 + C_2 e^\eta + C_3 e^{-\eta}, \quad (26)$$

Convergence of the homotopy solutions

It is now a well established argument that the convergence of series solutions (22) and (23) depends upon the auxiliary parameters h . The admissible range of values of h_f and h_θ (for some fixed values of parameters) lie along the line segment parallel to h_f and h_θ - axes. For example in Figs. 2 and 3 the permissible range of values of h_f and h_θ are

Table 3. Values of heat transfer characteristics at wall $-\theta'(0)$ for different emerging parameters when $\bar{h}_f = -0.8$ and $\bar{h}_\theta = -0.7$.

α	Γ	β	ε	G	R	Pr	A	$-(1+\frac{4}{3}R)\theta'(0)$
0.0								1.35702
$\pi/6$								1.35798
$\pi/3$								1.34926
$\pi/4$	0.0							1.69881
	0.4							1.72556
	0.7							1.74109
	0.9							1.74984
		0.0						1.71555
		0.5						1.71319
		0.9						1.71114
			0.0					1.10162
			0.4					1.61674
			0.6					1.71319
				0.0				1.69868
				0.5				1.72227
				0.8				1.73515
					0.0			1.54046
					0.3			1.71319
					0.6			2.00303
						1.2		1.91058
						1.5		2017721
						1.9		2049323
							-0.1	1.80783
							0.0	1.76059
							0.1	1.71319

doi:10.1371/journal.pone.0103214.t003

$-1.26 \leq h_f \leq -0.24$ and $-1.4 \leq h_\theta \leq -0.25$ respectively when $\varepsilon = 0.6$. This series solutions converge for the whole region of η when $h_f = -0.9$ and $h_\theta = -0.8$. Table 1. shows the convergence of HAM solution for different order of approximations. It is clear from this table that 10^{th} order of approximations are sufficient for convergent solutions up to six decimal place.

Results and Discussion

This section examines the effects of different physical parameters on the velocity and temperature fields. Hence Figs. (4, 5, 6, 7, 8, 9, 10, 11, 12, 13, 14, 15, 16) are plotted. Fig. 4 elucidates the behavior of inclination angle α on the velocity and the boundary layer thickness. $\alpha = 0$ shows the corresponding velocity profiles in the case of a vertical sheet for which the fluid experiences the maximum gravitational force. On the other hand when α changes from 0 to $\pi/2$ i.e. when the sheet moves from vertical to horizontal direction, the strength of buoyancy force decreases and consequently the velocity and the boundary layer thickness decrease. Fig. 5 indicates that velocity field f' is an increasing function of G . This is because a larger value of G accompanies a stronger buoyancy force which leads to an increase in the x -component of velocity. The boundary layer thickness also increases with an increase in G . Variation in f' with an increase in β can be seen from Fig. 6. It is noticed that f' decreases and boundary layer thins when β is increased. Influence of unsteady parameter ε on the velocity field is displayed in Fig. 7. Increasing values of ε indicates smaller stretching rate in the x -direction which eventually decreases the boundary layer thickness. Interestingly the velocity increases by increasing ε at sufficiently large distance from the sheet. Variation in the x -component of velocity with an increase in the fluid parameter Γ can be described from Fig. 8. In accordance with Mushtaq et al. [25], the velocity field f' increases with an increase in Γ .

Radiation effects on the velocity and temperature distributions are perceived from Figs. 9 and 10. An increase in R enhances the heat flux from the sheet which gives rise to the fluid's velocity and temperature. Wall slope of the temperature function therefore increases with an increase in R . Fig. 11 portrays the effect of Prandtl number on the thermal boundary layer. From the definition of Pr given in Eq. (10), it is obvious that increasing values of Pr decreases conduction and enhances pure convection or the transfer of heat through unit area. That is why temperature and the thermal boundary layer thickness decrease with an increase in Pr . This reduction in the thermal boundary layer accompanies a larger heat transfer rate from the sheet. Temperature profiles for different values of Γ are shown in Fig. 12. It is seen that temperature θ is an increasing function of Γ . Fig. 13 indicates that an increase in the strength of buoyancy force due to temperature gradient decreases the temperature and the thermal

References

- Wang CY (1990) Liquid film on an unsteady stretching surface. Q. Appl. Math. 48: 601–10.
- Andersson HI, Aarseth JB, Dandapat BS (1996) Heat transfer in a liquid film on an unsteady stretching surface. J. Non-Newtonian Fluid Mech. 62: 1–8.
- Elbashbeshy EMA, Bazid MAA (2004) Heat transfer over an unsteady stretching surface. Heat Mass Transfer. 41: 1–4.
- Ishak A, Nazar R, Pop I (2009) Boundary layer flow and heat transfer over an unsteady stretching vertical surface. Meccanica. 44: 369–75.
- Abd El-Aziz M (2009) Radiation effect on the flow and heat transfer over an unsteady stretching sheet. Int. Commun. Heat Mass Transfer. 36: 521–524.
- Shateyi S, Motsa SS Thermal radiation effects on heat and mass transfer over an unsteady stretching surface. Mathem. Prob. Eng. DOI 10.1155/2009/965603.
- Tsai R, Huang KH, Huang JS (2008) Flow and heat transfer over an unsteady stretching surface with non-uniform heat source. Int. Commun. Heat Mass Transfer. 35: 1340–1343.
- Mukhopadhyay S (2009) Unsteady boundary layer flow and heat transfer past a porous stretching sheet in presence of variable viscosity and thermal diffusivity. Int. J. Heat Mass Transfer. 52: 5213–5217.
- Hayat T, Mustafa M (2010) Influence of thermal radiation on the unsteady mixed convection flow of a Jeffrey fluid over a stretching sheet. Z. Naturforsch. 65a: 711–719.
- Hayat T, Mustafa M, Hendi AA (2011) Time-dependent three-dimensional flow and mass transfer of elasto-viscous fluid over unsteady stretching sheet. Appl. Math. Mech. 32: 167–178.
- Mukhopadhyay S (2013) Effects of thermal radiation and variable fluid viscosity on stagnation point flow past a porous stretching sheet. Meccan. 48: 1717–1730.
- Bhattacharyya K (2013) MHD stagnation-point flow of Casson fluid and heat Transfer over a stretching sheet with thermal radiation. J. Thermodyn. DOI:10.1155/2013/169674.

boundary layer thickness. Influence of heat source/sink parameters on the thermal boundary layer are presented in Figs. 14 and 15. As expected the larger heat source (corresponding to $A > 0$ and $B > 0$) rises the fluid's temperature above the sheet. While the non-uniform heat sink corresponding to $A < 0$ and $B < 0$ can contribute in quenching the heat from stretching sheet effectively. Fig. 16 depicts that temperature θ is a decreasing function of the unsteady parameter ε .

Table 2 shows comparison of present work with Tsai et al. in a special case. A very good agreement is found between the results of wall temperature gradient. Table 3 shows the effect of embedded parameters on heat transfer characteristics at the wall $-\theta'(0)$. Since in the present case the sheet is hotter than the fluid i.e. $T_w > T_\infty$ thus heat flows from the sheet to the fluid and hence $\theta'(0)$ is negative. From this table we observe that with an increase in α , β and R the wall heat transfer rate $|\theta'(0)|$ decreases. However it increases when Γ , ε and Pr are increased.

Conclusions

This article addressed the radiation effects in the unsteady boundary layer flow of Powell-Eyring fluid past an unsteady inclined stretching sheet with non-uniform heat source/sink. Homotopy analysis method (HAM) was used to obtain approximate analytic solutions of the governing nonlinear problem. The important findings are listed below.

- The strength of gravitational force can be varied by changing the inclination angle α which the sheet makes with the vertical direction. The velocity decreases with an increase in α .
- Velocity field f' and temperature θ are decreasing function of the unsteady parameter ε .
- Velocity increases and temperature decreases when the fluid parameter Γ is increased.
- Increase in the radiation parameter R enhances the heat flux from the plate which increases the fluid's velocity and temperature.
- The analysis for the case of viscous fluid can be obtained by choosing $\Gamma = \beta = 0$. Further the results for horizontal stretching sheet are achieved for $\alpha = \pi/2$.

Author Contributions

Conceived and designed the experiments: TH SA MM AA. Performed the experiments: TH SA MM AA. Analyzed the data: TH SA MM AA. Contributed reagents/materials/analysis tools: TH SA MM AA. Wrote the paper: TH SA MM AA.

13. Yang X-J, Baleanu D (2013) Fractal heat conduction problem solved by local fractional variation iteration method. *Thermal Sci.* 17: 625–628.
14. Yang Ali-Min, Cattani C, Zhang Ce, Xie G, Yang X-J (2014) Local Fractional Fourier Series Solutions for Non-homogeneous Heat Equations Arising in Fractal Heat Flow with Local Fractional Derivative. *Advan. Mech. Eng.* 2014: 5.
15. Harris J (1977) *Rheology and non-Newtonian flow*, Longman.
16. Bird RB, Curtiss CF, Armstrong RC, Hassager O (1987) *Dynamics of polymeric liquids*. Wiley.
17. Powell RE, Eyring H (1944) *Nature*, London.
18. Eldabe NTM, Hassan AA, Mohamed MAA (2003) Effect of couple stresses on the MHD of a non-Newtonian unsteady flow between two parallel porous plates. *Z. Naturforsch.* 58a: 204–210.
19. Zucco J, Beg OA (2009) Network numerical simulation applied to pulsatile non-Newtonian flow through a channel with couple stress and wall mass effects. *Int. J. Appl. Math. and Mech.* 5: 1–16.
20. Islam S, Shah A, Zhou CY, Ali I (2009) Homotopy perturbation analysis of slider bearing with Powell-Eyring fluid. *Z. Angew. Math. Phys.* 60: 1178–1193.
21. Patel M, Timol MG (2009) Numerical treatment of Powell—Eyring fluid flow using method of satisfaction of asymptotic boundary conditions. *Appl. Num. Math.* 59: 2584–2592.
22. Hayat T, Iqbal Z, Qasim M, Obaidat S (2012) Steady flow of an Eyring-Powell fluid over a moving surface with convective boundary conditions. *Int. J. Heat Mass Transfer.* 55: 1817–1822.
23. Mushtaq A, Mustafa M, Hayat T, Rahi M, Alsaedi A (2013) Exponentially stretching sheet in a Powell-Eyring fluid: Numerical and series solutions. *Z. Naturforsch.* 68a: 791–798.
24. Khader MM, Megahed AM (2013) Numerical studies for flow and heat transfer of the Powell-Eyring fluid thin film over an unsteady stretching sheet with internal heat generation using the chebyshev finite difference method. *J. Applied Mechanics Technical Phys.* 54: 440–450.
25. Zaman H (2013) Unsteady Incompressible Couette Flow Problem for the Eyring-Powell Model with Porous Walls. *American J. Computational Math.* 3: 313–325.
26. Liao S (2010) An optimal homotopy-analysis approach for strongly nonlinear differential equations. *Commun. Nonlinear Sci. Num. Simul.* 15: 2003–2016.
27. Abbasbandy S, Shivanian E, Vajravelu K (2011) Mathematical properties of h-curve in the frame work of the homotopy analysis method. *Commun. Nonlinear Sci. Numer. Simul.* 16: 4268–4275.
28. Hashmi MM, Hayat T, Alsaedi A (2012) On the analytic solutions for squeezing flow of nanofluid between parallel disks. *Nonlinear Anal. Model. Control* 17: 418–430.
29. Mustafa M, Hina S, Hayat T, Ahmad B (2013) Influence of induced magnetic field on the peristaltic flow of nanofluid. *Meccan.* DOI:10.1007/s11012-013-9809-5.
30. Mustafa M, Farooq MA, Hayat T, Alsaedi A (2013) Numerical and series solutions for stagnation-point flow of nanofluid over an exponentially stretching sheet. *PLoS ONE.* DOI:10.1371/journal.pone.0061859.
31. Mustafa M, Hayat T, Obaidat S (2013) Boundary layer flow of a nanofluid over an exponentially stretching sheet with convective boundary conditions. *Int. J. Num. Meth. Heat & Fluid Flow.* 23: 945–959.
32. Rashidi MM, Abelman S, Mehr FN (2013) Entropy generation in steady MHD flow due to a rotating disk in a nanofluid. *Int. J. Heat Mass Transfer.* 62: 515–525.
33. Rashidi MM, Bég OA, Kavyani N, Islam MN Entropy generation in hydromagnetic convective Von Karman swirling flow: Homotopy Analysis. *Int. J. Applied Math. Mech.* (In press).
34. Turkyilmazoglu M, Pop I (2013) Heat and mass transfer of unsteady natural convection flow of some nanofluids past a vertical infinite flat plate with radiation effect. *Int. J. Heat Mass Transfer.* 59: 167–171.
35. Turkyilmazoglu M, Pop I (2013) Exact analytical solutions for the flow and heat transfer near the stagnation point on a stretching/shrinking sheet in a Jeffrey fluid. *Int. J. Heat Mass Transfer.* 57: 82–88.
36. Brewster MQ (1972) *Thermal radiative transfer properties*. John Wiley and Sons, New York.
37. Sparrow EM, Cess RD (1978) *Radiation heat transfer*, Hemisphere, Washington.
38. Raptis A (1998) Radiation and free convection flow through a porous medium. *Int. Commun. Heat Mass Transfer.* 25: 289–295.
39. Rahman MM, Uddin MJ, Aziz A (2009) Effect of variable electrical conductivity and non-uniform heat source (or sink) on convective micropolar fluid flow along an inclined flat plate with surface heat flux. *Int. J. Therm. Sci.* 48: 2331–2340.
40. Nandeppanavar MM, Vajravelu K, Abel MS, Ng C (2011) Heat transfer over a nonlinearly stretching sheet with non-uniform heat source and variable wall temperature. *Int. Comm. Heat Mass Transfer.* 54: 4960–4965.